

Influence of Glycyl-L-Glutamic Acid Dipeptide on Calcium Pyrophosphate Dihydrate Crystallization

Polat, Sevgi; An, Qi; Eral, Huseyin Burak

DOI

[10.1002/ceat.202200628](https://doi.org/10.1002/ceat.202200628)

Publication date

2023

Document Version

Final published version

Published in

Chemical Engineering and Technology

Citation (APA)

Polat, S., An, Q., & Eral, H. B. (2023). Influence of Glycyl-L-Glutamic Acid Dipeptide on Calcium Pyrophosphate Dihydrate Crystallization. *Chemical Engineering and Technology*, 46(11), 2301-2309. <https://doi.org/10.1002/ceat.202200628>

Important note

To cite this publication, please use the final published version (if applicable). Please check the document version above.

Copyright

Other than for strictly personal use, it is not permitted to download, forward or distribute the text or part of it, without the consent of the author(s) and/or copyright holder(s), unless the work is under an open content license such as Creative Commons.

Takedown policy

Please contact us and provide details if you believe this document breaches copyrights. We will remove access to the work immediately and investigate your claim.

Sevgi Polat^{1,2,*}
Qi An¹
Huseyin Burak Eral¹

Influence of Glycyl-L-Glutamic Acid Dipeptide on Calcium Pyrophosphate Dihydrate Crystallization

The increasing prevalence of calcium pyrophosphate dihydrate (CPPD) deposition disease, a form of arthritis with high inflammatory potential, has triggered considerable interest in the search for additives to prevent CPPD crystal formation, particularly in the field of biomineralization. In this context, CPPD crystallization in aqueous solution with and without glycine, glutamic acid, or glycyl-L-glutamic acid as crystal-growth modifier was experimentally investigated. The produced crystals were characterized structurally, morphologically, and in terms of their surface charge. In addition, the thermal degradation profiles of CPPD crystals obtained with and without the modifiers were characterized by TGA-FTIR, and the major volatile product was H₂O.

Keywords: Calcium pyrophosphate dihydrate, Crystallization, Morphology, Peptides, Thermogravimetric analysis

Received: December 27, 2022; revised: March 03, 2023; accepted: May 24, 2023

DOI: 10.1002/ceat.202200628

This is an open access article under the terms of the Creative Commons Attribution License, which permits use, distribution and reproduction in any medium, provided the original work is properly cited.



Supporting Information
available online

1 Introduction

The deposition of calcium pyrophosphate dihydrate (CPPD) crystals in synovial fluid or tissues causes arthritis or “pseudogout”. These crystal deposits can cause significant morbidity and are often underdiagnosed [1–6]. The disease is idiopathic in most patients; however, it has been associated with aging, osteoarthritis, gout, hyperparathyroidism, and metabolic disorders such as hemochromatosis and hypomagnesemia [7–10]. Although it mainly presents in the elderly, arthritis caused by these crystals is the third most common form of inflammatory arthritis [11]. Despite its prevalence, the etiology of CPPD disease is unclear with no specific therapies to alleviate it. The clinical protocols used have not inhibited the formation of CPPD crystals and inflammation, and pain relief has been limited [12]. To create new methods by which to inhibit crystal formation and develop an effective therapeutic protocol, CPPD etiology must be identified. Studies on CPPD precipitation in the presence of various additives are limited [13–18] and exactly how additives alter CPPD crystal formation is still an open question. An improved understanding of how additives inhibit CPPD crystal formation may inform the development of treatment methods for CPPD disease and may even inspire designer additives [19].

The objective of this study was to synthesize CPPD crystals in vitro by using a well-stirred reactor under pH- and temperature-controlled conditions to determine the effect of two amino acid modifiers – glycine (Gly) and glutamic acid (Glu) – and a dipeptide modifier – glycyl-L-glutamic acid (Gly-Glu) – on the CPPD crystallization process. Because information on the onset of CPPD formation was lacking, the study did not focus

on mimicking the in vivo conditions for CPPD polymorph precipitation but aimed only to evaluate and compare the effects of Gly, Glu, and Gly-Glu while keeping all the other synthetic parameters identical to the reference synthesis of triclinic (t)-CPPD without modifiers. The effect of Gly, Glu, and Gly-Glu was thoroughly investigated by X-ray diffraction (XRD), Fourier transform infrared (FTIR) spectroscopy, Raman spectroscopy, scanning electron microscopy (SEM), zeta potential measurement, and thermogravimetric analysis (TGA).

2 Experimental Section

2.1 Materials

Calcium chloride dihydrate (CaCl₂·2H₂O) and sodium pyrophosphate decahydrate (Na₄P₂O₇·10H₂O) were purchased from Merck (Darmstadt, Germany) and used without further purification. Glycine, L-glutamic acid, and glycyl-L-glutamic

¹Dr. Sevgi Polat <https://orcid.org/0000-0002-0934-2125>
(S.Polat@tudelft.nl, sevgi.polat@marmara.edu.tr),
Qi An, Dr. Huseyin Burak Eral

<https://orcid.org/0000-0003-3193-452X>

Process & Energy Department, Faculty of Mechanical, Maritime and Materials Engineering, Delft University of Technology, 2628 CB Delft, The Netherlands.

²Dr. Sevgi Polat
Chemical Engineering Department, Faculty of Engineering, Marmara University, 34854 İstanbul, Turkey.

acid (Gly-Glu) were obtained from Sigma-Aldrich (Gillingham, UK). Ultrapure water was used to prepare the solutions.

2.2 Experimental Methods

The study was conducted by using a 500-mL double-jacketed crystallizer at 90 °C and 400 rpm. A mechanical stirrer equipped with a three-bladed propeller was mounted in the center of the crystallizer, and a thermostat with an accuracy of 0.1 °C was used to control the temperature. A pH meter was attached to an automated pH control unit to monitor and maintain pH 4.0 by using 0.1 M HCl (aq) and NaOH (aq).

First, 250 mL of aqueous CaCl₂ solution was added to the crystallizer and allowed to reach the setting temperature. Once the temperature was stabilized, specific amounts of Gly, Glu, or Gly-Glu, ranging from 0 to 1.0 mM, were added to the CaCl₂ solution, after which 250 mL of Na₄P₂O₇ solution was added to the crystallizer at 3.0 mL min⁻¹ by using a peristaltic pump, and the mixture was continuously stirred to create a suspension. At all times, the crystallizer cover was kept closed. Once the reactant-feeding process was completed, the suspension was filtered by using a vacuum extraction flask with a 0.45-μm Millipore membrane filter. The obtained crystals were washed with ultrapure water and dried for further characterization.

2.3 Analysis

XRD was used to identify the crystal structure of the products. The diffraction patterns of solid samples were recorded with a Bruker D2 Phaser table-top X-ray powder diffractometer. Measurements were taken in the 2θ range of 10–70° at 30 kV and 10 mA. Raman spectra were collected with a Renishaw Raman InVia Reflex microscope in the wavenumber range between 400 and 1250 cm⁻¹ and provided information on the structure of the crystals. Attenuated total reflection FTIR (Shimadzu IR Affinity-1) analysis was used to determine the functional groups of the crystals. The resolution was 4 cm⁻¹ and 32 scans were acquired for each spectrum. Each sample was analyzed with at least three replicates. The crystal morphology was observed by SEM (Zeiss EVO LS 10). The image analysis software used a predefined scale to calculate the length and width of the samples. To improve the accuracy of the results, the calculation used at least 100 crystal samples and different SEM images of each sample. The zeta potential analysis was performed by using a Malvern Zetasizer Nano ZS (Malvern Instruments) to measure the surface charge of the crystals. Thermal degradation of the crystals prepared with and without additives and the gases evolved during TGA measurements were investigated with a thermogravimetric analyzer (TA Instruments SDT Q600) coupled with an FTIR spectrometer (Bruker Tensor27) simultaneously. The experiments were conducted at a heating rate of 20 °C min⁻¹ between 30 and 900 °C at a nitrogen flow rate of 50 mL min⁻¹. FTIR measurements were performed in the continuous scan mode for detecting volatiles, and the spectra were recorded in the range of 400–4000 cm⁻¹. The dehydration kinetic and thermodynamic calculations for CPPD crystals were conducted at heating rates of 5, 10, and 20 °C min⁻¹.

3 Results and Discussion

3.1 XRD, Raman, and FTIR Analyses

The effects of each additive and its varying concentrations on the crystal structure were investigated by XRD, Raman spectroscopy, and FTIR spectroscopy (Fig. 1). The XRD patterns (Fig. 1a) indicated that the crystallization process formed only t-CPPD crystals with space group *P1* without other crystalline phases or phase transformation, which indicated that the presence of Gly, Glu, and Gly-Glu in the studied concentration ranges had no effect on crystal type. The main characteristic peaks of t-CPPD were identified at 10.9, 12.7, 16.9, 22.0, 25.7, 27.5, 33.3, and 39.7°, which were indexed to the (010), (100), (110), (020), (120), (210), (030), and (311) crystal faces, respectively. The unit cell parameters of the CPPD crystals obtained in pure media were calculated to be $a = 7.361 \text{ \AA}$, $b = 8.287 \text{ \AA}$, $c = 6.699 \text{ \AA}$, $\alpha = 102.83^\circ$, $\beta = 72.71^\circ$, and $\gamma = 94.98^\circ$. These results agreed with those reported in earlier studies [3, 15].

Raman and FTIR analyses were conducted to further identify the presence and extent of certain groups on the CPPD surface. As shown in Fig. 1b, the Raman spectra were not significantly changed after adding Gly, Glu, and Gly-Glu to the crystallization media within the accuracy of the method. In addition, the characteristic peaks of each additive were not observed compared with those of the pure CPPD crystals. This indicated that the additives interacted with CPPD crystals only through physical adsorption instead of forming chemical bonds, which was also consistent with FTIR analyses. In Fig. 1c, the broad absorption peak between 3600 and 2800 cm⁻¹ is a characteristic indicator of the water O–H stretching vibration, and the peak at ca. 1650 cm⁻¹ belongs to the O–H plane-bending vibration. Moreover, the peaks between 1250 and 1000 cm⁻¹ were attributed to the P–O stretching vibrations. The peaks ranging from 1000 and 700 cm⁻¹ were associated with the P–O–P stretching vibrations in the CPPD crystals [13, 20]. Meanwhile, there were no new peaks other than those characteristic of the dihydrate form, which demonstrated that neither the amino acids nor Gly-Glu peptide formed new chemical bonds with CPPD. In other words, all additives interacted primarily with the surfaces of the CPPD crystals through physical adsorption and not through chemical bonding. Consequently, it is hypothesized that additives may inhibit the crystallization process by occupying the active sites on those surfaces.

3.2 SEM Analysis

Fig. 2 shows the morphological characteristics of the t-CPPD crystals obtained as a result of the reaction between CaCl₂ and Na₄P₂O₇ with and without additives. As shown in Fig. 2a, the CPPD crystals obtained without the additives had an elongated plank-like shape [3, 15] which is consistent with the results in the literature, with an agglomeration tendency and unorganized distribution. SEM image also revealed that the crystals grew in a layered pattern. Fig. 3a shows the variation in width and length for the CPPD crystals obtained with and without modifiers. As shown in Fig. 3a, the average length and width of the CPPD crystals were 50.10 ± 5.8 and $10.52 \pm 2.9 \mu\text{m}$,

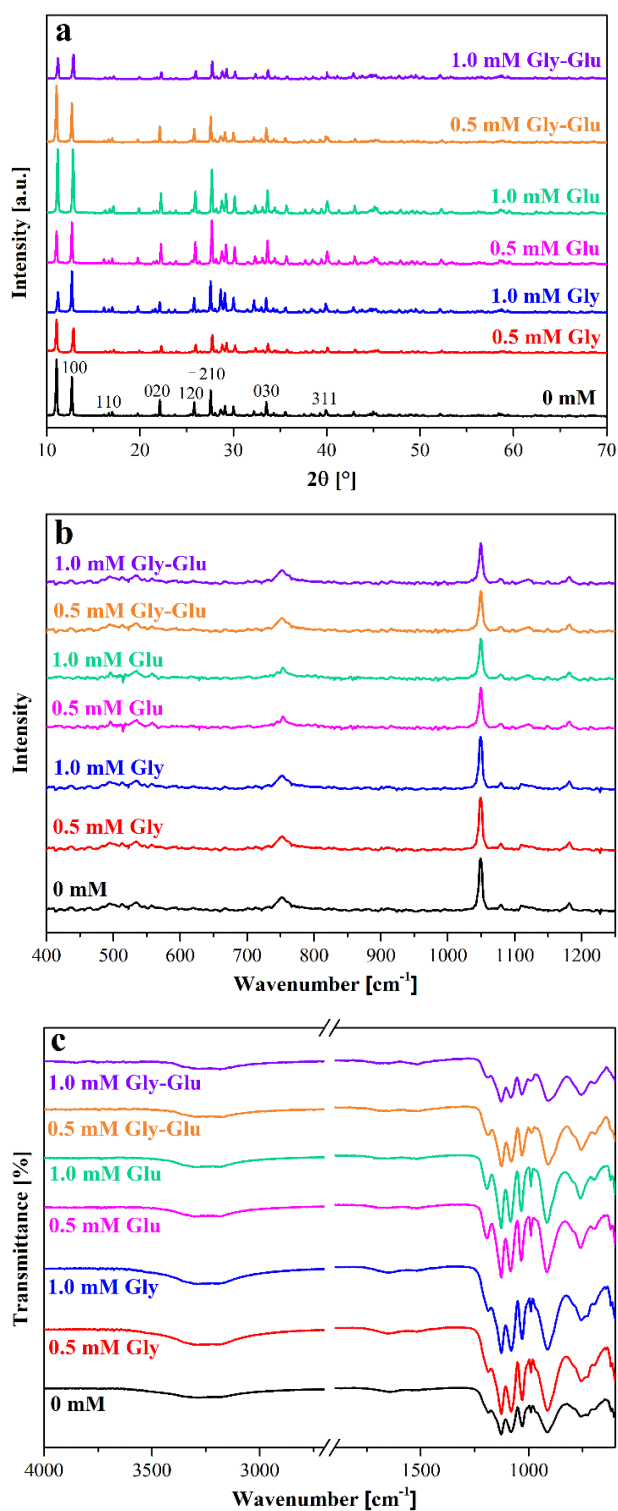


Figure 1. (a) XRD patterns, (b) Raman spectra, and (c) FTIR spectra of the CPPD crystals obtained at different concentrations of Gly, Glu, and Gly-Glu.

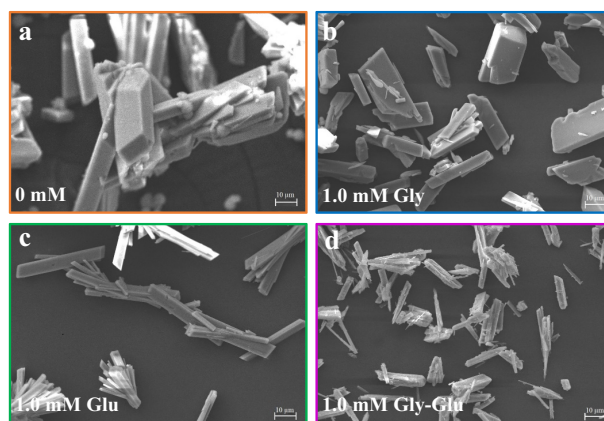


Figure 2. SEM images of the CPPD crystals obtained in aqueous solution with (a) 0 mM additive, (b) 1.0 mM Gly, (c) 1.0 mM Glu, and (d) 1.0 mM Gly-Glu.

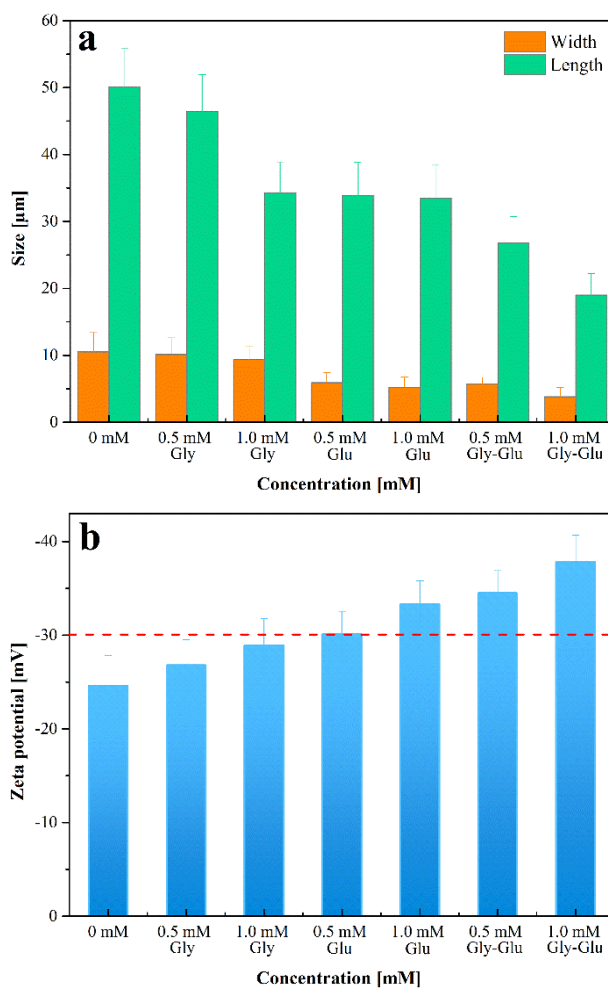


Figure 3. (a) Variation in width and length of the CPPD crystals obtained at different concentrations of Gly, Glu, and Gly-Glu. (b) Zeta potentials of the CPPD crystals as a function of Gly, Glu, and Gly-Glu concentrations.

respectively. Not only the shapes but also the sizes of the CPPD crystals were altered upon the addition of additives. A low concentration (0.5 mM) of Gly (Fig. S1 in the Supporting Information) only slightly modified the shape and size of the CPPD crystals. The crystals grew on top of each other in an irregular and a heterogeneous manner and created irregularities and defects on the crystal surfaces. When the concentration of Gly was increased from 0.5 to 1.0 mM, a slight decrease in agglomeration was observed (Fig. 2b). To better observe the effects of Glu on the morphology of the CPPD crystals, the studies were conducted at two different concentrations, as with Gly. An overall look at the obtained CPPD crystals showed that thinner, good-quality crystals formed in the presence of Glu compared with pure media. Although the CPPD crystals obtained at high concentration resembled those obtained at the low concentration, they had a lower tendency to agglomerate. After increasing the concentration of Glu, rod-like crystals with a more uniform, homogenous, and smooth surface were obtained (Fig. 2c). Concurrently, compared with pure media, the average particle size of the crystals and their tendency for agglomeration decreased. In addition, the crystal width decreased by ca. 50% with 1.0 mM Glu compared with pure media (Fig. 3a).

Figs. S1c and 2d show SEM images of the crystals obtained in the presence of 0.5 and 1.0 mM Gly-Glu, respectively. The obtained CPPD crystals were less agglomerated, thinner, and smaller than those obtained with other additives. They did not have a robust structure with high modulus and tended to break under the hydrodynamic conditions in the crystallizer. The surfaces of these crystals were rough with irregularities and defects, possibly through secondary heterogeneous nucleation on their surfaces. That is, loosely structured crystals were replaced by thinner crystals with a less compact structure.

In the morphological assessments, Gly-Glu as additive has a more obvious effect than Gly and Glu additives. Although Gly and Glu slightly changed the agglomeration tendency of the CPPD crystals, Gly-Glu provided a substantial decrease in, and nearly eliminated this tendency. Concentrically growing crystals with a more compact structure formed in the presence of Gly and Glu, whereas sparsely distributed, homogeneous, and independently growing crystals of a smaller particle size were observed in the presence of Gly-Glu. These morphological changes may have originated from adsorption of the additives on the surface of the CPPD crystals, which may have inhibited calcium and pyrophosphate deposition or selectively hindered the growth of particular crystal faces. Even though the experiments were performed in aqueous solution media, the effects of the used additives may be different in the human body due to the different solution chemistry and presence of macromolecules, as previously observed in the literature [21, 22]. The solution chemistry of the human environment may alter the conformations of used additives and change how these additives interact with CPPD crystals. Yet without detailed solution chemistry modeling considering the role of the used additives in solution chemistry, which is beyond the scope of this study, the underlying physical mechanism of CPPD crystallization remains an open question.

3.3 Zeta Potential Analysis

In addition to the structural and morphological properties of the crystals, their surface characteristics were identified by measuring the zeta potential to obtain information on the interaction between the additives and the CPPD crystals in aqueous solution. The zeta potential determines the colloidal stability of a solution, and the zeta potentials of the crystals obtained with and without modifiers are shown in Fig. 3b. The CPPD crystals obtained in pure media had a zeta potential of -24.6 ± 3.2 mV, and we observed that the influence of all modifiers used on the zeta potential was significant. The zeta potential results indicated that the CPPD crystals obtained under all studied conditions with additives exhibited a negatively charged surface. Increasing the concentration of all additives used in the crystallization made the zeta potential more negative due to the crystal surface being covered with the negatively charged ions of the additives. The CPPD crystals obtained in 1.0 mM Gly and Glu had zeta potentials of -28.9 ± 2.9 and -33.3 ± 2.5 mV, respectively. The results indicate that Gly and Glu changed the physicochemical properties of the CPPD crystals to some extent, thus affecting their agglomeration and shape. A similar outcome was observed for the CPPD crystals obtained with Gly-Glu. The addition of Gly-Glu resulted in a significant reduction in the surface charge, and increasing its concentration remarkably increased this value, making the surface more negatively charged (-37.8 ± 2.9 mV). This variation may suggest that van der Waals interactions induced adsorption of the additives on the CPPD crystal surfaces.

3.4 TGA-FTIR Analyses

The effects of Gly, Glu, and Gly-Glu on the thermal degradation behaviors of the CPPD crystals were studied by TGA-FTIR. Fig. S2 shows the TGA-derivative thermogravimetry (DTG) curves of the crystals in the temperature region between 30 and 900 °C. The weight loss of the CPPD crystals obtained without the modifier was 12.6% at 900 °C, which was close to the theoretical value (12.4%). There are three stages in the thermal degradation of t-CPPD crystals: loss of ca. 50% of an H₂O molecule, loss of one H₂O molecule, and formation of a dehydrated β -Ca₂P₂O₇ phase, respectively [23]. As shown in Figs. S2b–d, Gly, Glu, and Gly-Glu had no significant effect on the thermal degradation mechanism and the degradation behavior was similar. The temperature ranges were also similar to those observed in pure media.

By using TGA-FTIR, a detailed understanding of the nature of the thermal degradation processes can be achieved. Fig. S3 shows the FTIR plots using Gram-Schmidt (GS) orthogonalization for the absorbance values of gases generated during thermal degradation at a heating rate of 20 °C min⁻¹. The plots follow the evolution of gases throughout the thermal degradation process. These GS profiles directly correlated with the stages in the TGA curves, and the emergence of peaks was compatible with the TG and DTG curves. Compared to the DTG curves, the only change observed was a small shift of the peak temperature in the GS curve toward a higher region, a consequence of the short time delay in the transport of the evolved volatile

substances from TGA to FTIR. Figs. 4a–d show the three-dimensional (3D) FTIR spectra of the crystals obtained with and without additives. The functional groups of the CPPD crystals, represented by each characteristic peak, can be identified from the 3D FTIR spectrum. As shown in Fig. 4, the evolving profile of volatile products during degradation is a function of both wavenumber and temperature. The dehydration of CPPD crystals mainly occurred from ca. 200 to 440 °C. Meanwhile, the main and most intense absorption peaks observed in the 3D FTIR spectrum, between ca. 3900 and ca. 3250 cm^{-1} , were attributed to the symmetric and asymmetric stretching vibrations of H_2O molecules, with the maximum peak at ca. 350 °C. In addition, the presence of H_2O molecules was also identified by the bands between ca. 1700 and ca. 1400 cm^{-1} . Based on TGA/FTIR results, water was the main volatile product that was evolved.

3.5 Kinetic and Thermodynamic Analyses

To determine the water of crystallization of the CPPD crystals, along with their thermodynamic degradation and kinetic parameters, such as activation energy and frequency factor, TGA was conducted. In general, TGA data can be analyzed by model-fitting or non-model-fitting methods to obtain isothermal or non-isothermal solid-state kinetic information. Model-

fitting methods subject data to various models and then select the model that provides the optimum statistical fit. Then, using this model, the activation energy and frequency factor are calculated. On the other hand, using model-free methods of kinetic analysis makes no assumptions about the reaction mechanism [24, 25]. In this study, four isoconversional kinetic methods, namely, the Flynn-Wall-Ozawa (FWO) [26, 27], Kissinger-Akahira-Sunose (KAS) [28, 29], Starink [30], and Friedman [31] models were used to determine the activation energies of the CPPD crystals. These methods are frequently employed and accepted for the evaluation of kinetic parameters. FWO, KAS, and Starink are integral methods, whereas Friedman is a differential method. Eqs. (1)–(4) show the linearized forms of the kinetic models which were used during the isoconversional kinetic analysis.

FWO:

$$\ln \beta = \ln \left(\frac{AE}{Rg(\alpha)} \right) - 5.331 - 1.052 \frac{E}{RT} \quad (1)$$

KAS:

$$\ln \left(\frac{\beta}{T^2} \right) = \ln \left(\frac{AR}{Eg(\alpha)} \right) - \frac{E}{RT} \quad (2)$$

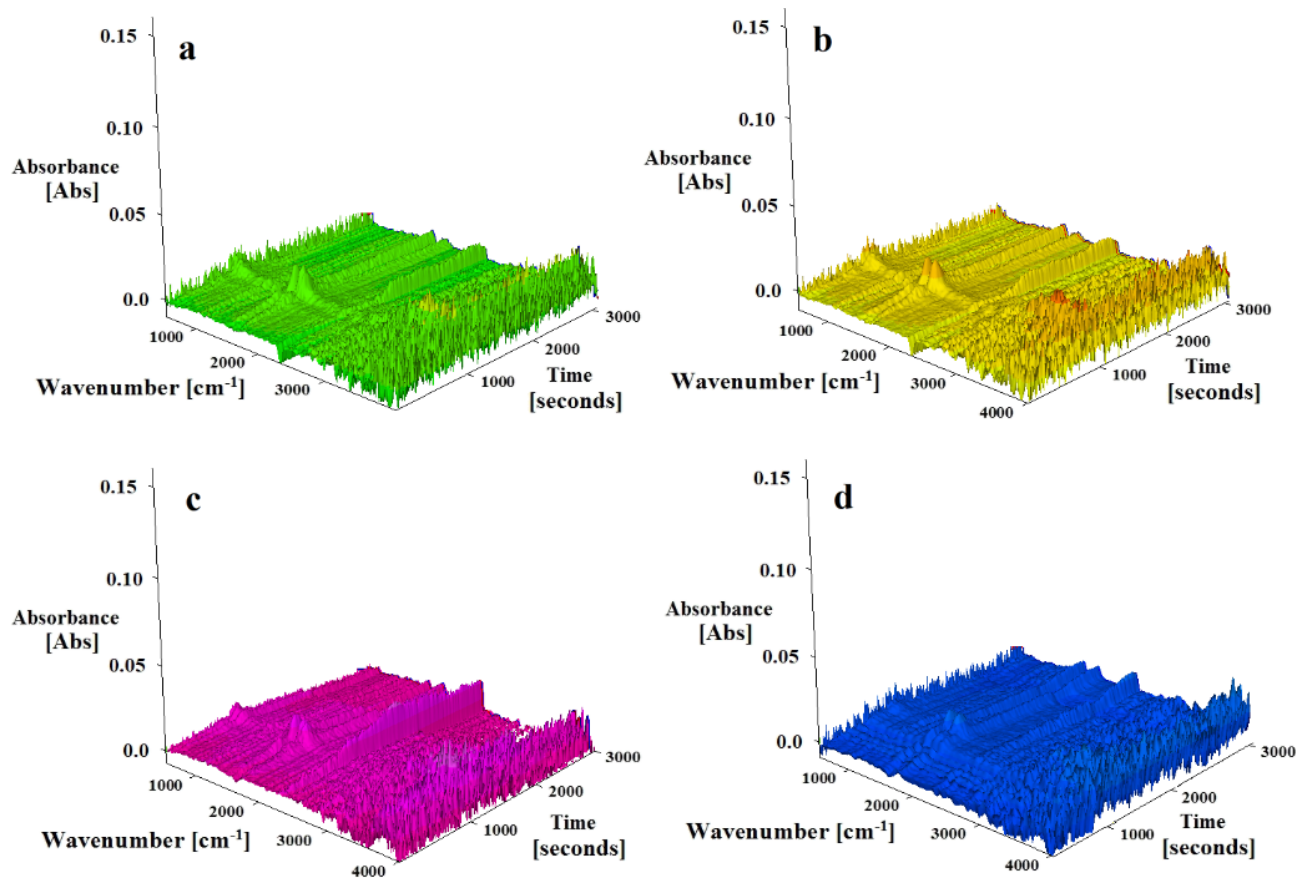


Figure 4. 3D FTIR spectra of the CPPD crystals obtained at (a) 0 mM additive, (b) 1.0 mM Gly, (c) 1.0 mM Glu, and (d) 1.0 mM Gly-Glu.

Starink:

$$\ln\left(\frac{\beta}{T^{1.92}}\right) = C - 1.0008 \frac{E}{RT} \quad (3)$$

Friedman:

$$\ln\left(\frac{d\alpha}{dt}\right) = \ln\left(\beta \left(\frac{d\alpha}{dT}\right)\right) = \ln[Af(\alpha)] - \frac{E}{RT} \quad (4)$$

where α ¹⁾ is the conversion, β the heating rate, $f(\alpha)$ is the reaction model, $g(\alpha)$ is the integrated reaction model, R is the ideal gas constant, t is time, T is the temperature.

The activation energies E from isoconversional methods can be employed to calculate the frequency factor A . To determine the frequency factor for each value of α , Kissinger's equation [32] as given in Eq. (5) was used in this study:

$$A = \frac{\beta E \exp(E/RT_{peak})}{RT_{peak}^2} \quad (5)$$

where T_{peak} is the temperature at the maximum conversion rate.

Based on the obtained activation energy and the frequency factor, the thermodynamic parameters of the CPPD crystals, including enthalpy change ΔH , Gibbs free energy change ΔG , and entropy change ΔS , can be estimated by using Eyring equations (Eqs. (6)–(8)) [33, 34]:

$$\Delta H = E - RT \quad (6)$$

$$\Delta G = E + RT_{peak} \ln\left(\frac{K_B T_{peak}}{hA}\right) \quad (7)$$

$$\Delta S = \frac{\Delta H - \Delta G}{T_{peak}} \quad (8)$$

where K_B is the Boltzmann constant and h the Planck constant.

In this study, data from TGA and DTG curves were used to calculate the dehydration kinetics and thermodynamic parameters of the CPPD crystals obtained in pure media by using the FWO, KAS, Starink, and Friedman methods. Fig. 5 shows the TGA and DTG curves of the CPPD crystals obtained at three different heating rates in the dehydration zone, which were accounted for in the calculation of the activation energy. The same dehydration trend was observed at all the heating rates used in this study on CPPD crystals. The dehydration temperature increased with increasing heating rate as a result of an increase in the subsequent thermal lag. The activation energy, which is the minimum amount of energy needed to start the process, was calculated on the basis of the slopes of the lines obtained with the FWO, KAS, Starink, and Friedman models in the range of $\alpha = 0.1$ – 0.9 in increments of 0.1 . The Arrhenius plots for the FWO, KAS, Starink, and Friedman models for the

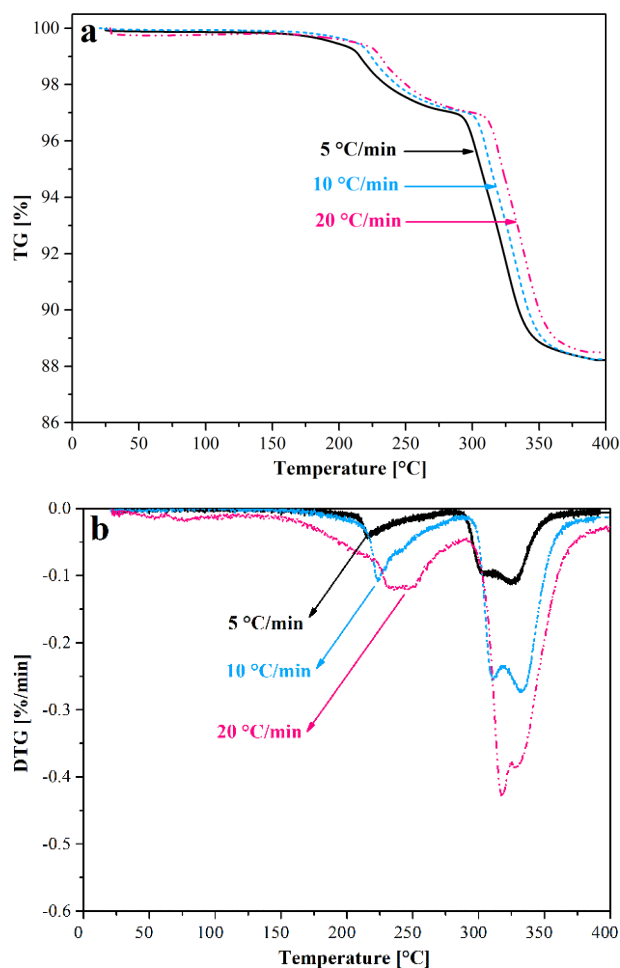


Figure 5. (a) TGA and (b) DTG curves of the CPPD crystals at different heating rates.

CPPD crystals (Fig. S4) all showed nearly parallel lines, and experimental data showed a good fit for each model.

Tab. 1 shows how the activation energy based on isoconversional models is dependent on the degree of conversion. All lines had correlation coefficients $R^2 > 0.985$, indicating accuracy and reliability of the calculated activation energies. Depending on the kinetic model that was applied, the activation energies for CPPD crystals were in the range between 174.5 and 270.5 kJ mol^{-1} , and the average values were 233.5, 236.0, 236.2, and 238.4 kJ mol^{-1} for the FWO, KAS, Starink, and Friedman models, respectively. The slight differences in activation energy could be related to the different approximations and calculations used to derive the isoconversional model equations. Meanwhile, the frequency factor of the crystals increased in parallel with the activation energy, and the range of these calculated values was between 8.58×10^{14} and $2.08 \times 10^{23} \text{ min}^{-1}$ (Tab. 2).

Meanwhile, the frequency factor of the crystals increased in parallel with the activation energy, and the range of these calculated values was between 8.58×10^{14} to $2.08 \times 10^{23} \text{ min}^{-1}$ (Tab. 2).

1) List of symbols at the end of the paper.

Table 1. Activation energies E [kJ mol^{-1}] with respect to conversion α for thermal degradation of CPPD crystals.

α	FWO		KAS		Starink		Friedman	
	E	R^2	E	R^2	E	R^2	E	R^2
0.1	177.6	0.9986	178.4	0.9985	178.6	0.9985	174.5	0.9854
0.2	193.9	0.9986	195.0	0.9876	195.2	0.9876	206.0	0.9922
0.3	215.0	0.9999	216.5	0.9999	216.7	0.9999	247.3	0.9996
0.4	230.8	0.9999	233.0	0.9999	233.2	0.9999	251.7	0.9955
0.5	241.6	0.9999	244.3	0.9999	244.5	0.9988	256.0	0.9999
0.6	250.1	0.9999	253.1	0.9999	253.3	0.9999	252.3	0.9962
0.7	259.4	0.9995	262.9	0.9995	263.1	0.9963	252.8	0.9920
0.8	266.6	0.9988	270.3	0.9963	270.5	0.9994	253.1	0.9902
0.9	266.7	0.9965	270.3	0.9988	270.5	0.9991	252.5	0.9853
Average	233.5		236.0		236.2		238.4	

Table 2. Thermodynamic parameters for thermal degradation of CPPD crystals at $20^\circ\text{C min}^{-1}$.

α	FWO				KAS				Starink				Friedman			
	A	ΔH	ΔG	ΔS	A	ΔH	ΔG	ΔS	A	ΔH	ΔG	ΔS	A	ΔH	ΔG	ΔS
0.1	1.63×10^{15}	172.6	152.9	32.0	1.92×10^{15}	173.4	152.9	33.4	2.00×10^{15}	173.5	152.9	33.7	8.58×10^{14}	169.4	153.0	26.7
0.2	4.38×10^{16}	188.8	152.5	59.4	5.41×10^{16}	191.2	152.5	63.2	5.63×10^{16}	190.1	152.5	61.5	4.94×10^{17}	200.9	152.2	79.5
0.3	3.03×10^{18}	209.9	152.0	94.6	4.11×10^{18}	212.7	151.9	99.2	4.29×10^{18}	211.6	151.9	97.5	1.98×10^{21}	242.2	151.3	148.5
0.4	7.24×10^{19}	225.7	151.6	121.0	1.13×10^{20}	229.2	151.6	126.8	1.18×10^{20}	228.1	151.6	125.1	4.81×10^{21}	246.6	151.2	155.9
0.5	6.36×10^{20}	236.5	151.4	139.0	1.09×10^{21}	240.5	151.3	145.7	1.14×10^{21}	239.4	151.3	143.9	1.14×10^{22}	250.9	151.1	163.1
0.6	3.48×10^{21}	245.0	151.2	153.2	6.41×10^{21}	249.3	151.1	160.4	6.65×10^{21}	248.2	151.1	158.6	5.46×10^{21}	247.2	151.2	156.9
0.7	2.28×10^{22}	254.4	151.0	168.8	4.53×10^{22}	259.1	150.9	176.6	4.72×10^{22}	258.0	150.9	174.8	5.95×10^{21}	247.7	151.1	157.6
0.8	9.49×10^{22}	261.5	150.9	180.7	2.00×10^{23}	266.5	150.8	189.0	2.08×10^{23}	265.4	150.8	187.2	6.34×10^{21}	248.0	151.1	158.2
0.9	9.72×10^{22}	261.6	150.9	180.9	2.00×10^{23}	266.5	150.8	189.0	2.08×10^{23}	265.4	150.8	187.2	5.63×10^{21}	247.4	151.2	157.2
Av.	1.26×10^{20}	228.4	151.6	125.6	5.03×10^{22}	232.0	151.5	131.5	5.23×10^{22}	231.1	151.5	129.8	24.61×10^{21}	233.4	151.5	133.7

After determining the thermal kinetics parameters, the thermodynamic parameters were assessed to provide more insight into the thermal degradation of CPPD crystals (Tab. 2).

The ΔH value is a crucial parameter in the evaluation of whether the adsorption process is endothermic or exothermic, and this evaluation was made on the basis of whether this value is positive or negative; positive values of ΔH indicated an endothermic dehydration process. The ΔH values varied between 169.4 and 265.4 kJ mol^{-1} with average values of 228.4, 232.0, 231.1, and 233.4 kJ mol^{-1} for the FWO, KAS, Starink, and Friedman models at $20^\circ\text{C min}^{-1}$, respectively. The positive values of ΔH indicated that the dehydration process was endothermic. The ΔS value was between 26.7 and 189.0 $\text{J mol}^{-1}\text{K}^{-1}$, and ΔG was within the range of 150.8 and 153.0 kJ mol^{-1} . For all conversions, the ΔG values obtained were positive, indicating that the reactions are non-spontaneous.

4 Conclusion

An in vitro study of how Gly, Glu, and Gly-Glu alter the structure, morphological variations, and thermal degradation of CPPD crystals was performed by XRD, Raman, FTIR, SEM, and TGA analyses. The XRD, Raman, and FTIR results showed that the crystalline products obtained with and without modifiers were t-CPPD. SEM analysis showed that all the additives used greatly influenced the shapes and sizes of the CPPD crystals; however, the most distinct effect occurred in the presence of Gly-Glu. The length and width of the CPPD crystals decreased from 50.10 ± 5.8 to $19.00 \pm 3.2 \mu\text{m}$ and from 10.52 ± 2.9 to $3.8 \pm 1.4 \mu\text{m}$, respectively, after adding Gly-Glu. Zeta potential analysis demonstrated that all additives changed the surface charge of the crystals, and the largest variation in the negative charge occurred in the presence of Gly-Glu. In

addition, the thermal degradation profiles of the CPPD crystals obtained with and without modifiers were studied simultaneously by using thermogravimetric analysis coupled with FTIR; the major volatile product was H₂O. FWO, KAS, Starink, and Friedman methods were successfully employed to investigate the kinetic and thermodynamic parameters of the CPPD crystals at different conversion levels. The activation energy varied between 174.5 and 270.5 kJ mol⁻¹. Finally, the present study provides a general impression of the modified crystal morphology and variation in the size of the CPPD crystals that resulted from using Gly, Glu, and Gly-Glu. It is suggested that these findings will contribute to the efforts in identifying additives that prevent the deposition of CPPD crystals and eliminate the diseases it causes.

Supporting Information

Supporting Information for this article can be found under DOI: <https://doi.org/10.1002/ceat.202200628>.

The authors have declared no conflict of interest.

Symbols used

A	[min ⁻¹]	frequency factor
E	[kJ mol ⁻¹]	activation energy
$f(\alpha)$	[-]	reaction model
$g(\alpha)$	[-]	integrated reaction model
ΔG	[kJ/mol]	Gibbs free energy change
h	[J Hz ⁻¹]	Planck constant
ΔH	[kJ/mol]	enthalpy change
K_B	[J K ⁻¹]	Boltzmann constant
R	[J mol ⁻¹ K ⁻¹]	gas constant
R^2	[-]	correlation coefficient
ΔS	[J mol ⁻¹ K ⁻¹]	entropy change
t	[min]	time
T	[K]	temperature
T_{peak}	[K]	temperature at the maximum conversion rate

Greek letters

α	[-]	conversion
β	[C min ⁻¹]	heating rate

Abbreviations

CPPD	calcium pyrophosphate dihydrate
DTG	derivative thermogravimetry
FTIR	Fourier transform infrared
FWO	Flynn-Wall-Ozawa
Glu	glutamic acid
Gly	glycine
Gly-Glu	glycyl-L-glutamic acid
GS	Gram-Schmidt
KAS	Kissinger-Akahira-Sunose
SEM	scanning electron microscopy
t-CPPD	triclinic calcium pyrophosphate dihydrate

TGA	thermogravimetric analysis
XRD	X-ray diffraction

References

- [1] M. Zell, T. Aung, M. Kaldas, A. K. Rosenthal, B. Bai, T. Liu, A. Ozcan, J. D. Fitzgerald, *Osteoarthritis Cartilage Open* **2021**, *3* (1), 100133. DOI: <https://doi.org/10.1016/j.jocarto.2020.100133>
- [2] M. Nashi, S. Yamamoto, K. Maeda, N. Taniike, S. Hara, *J. Oral Maxillofac. Surg. Med. Pathol.* **2022**, *34* (1), 49–54. DOI: <https://doi.org/10.1016/j.ajoms.2021.06.007>
- [3] O. L. Katsamenis, N. Bouropoulos, in *Mineral Scales and Deposits* (Eds: Z. Amjad, K. D. Konstantinos), Elsevier, Amsterdam **2015**.
- [4] C. J. Williams, A. K. Rosenthal, *Best Pract. Res., Clin. Rheumatol.* **2021**, *35* (4), 101718. DOI: <https://doi.org/10.1016/j.berh.2021.101718>
- [5] J. Jung, J. Bong, S. J. Lee, M. Kim, J. S. Sung, M. Lee, M. Kang, J. Song, J. Jose, J. Pyun, *ACS Appl. Bio Mater.* **2021**, *4*, 3388–3397. DOI: <https://doi.org/10.1021/acsabm.0c01680>
- [6] D. C. Bassett, T. E. Robinson, R. J. Hill, L. M. Grover, J. E. Barralet, *Biomater. Adv.* **2022**, *140*, 213086. DOI: <https://doi.org/10.1016/j.bioadv.2022.213086>
- [7] K. Parperis, E. Papachristodoulou, L. Kakoullis, A. K. Rosenthal, *Semin. Arthritis Rheum.* **2021**, *51* (1), 84–94. DOI: <https://doi.org/10.1016/j.semarthrit.2020.10.005>
- [8] S. Cui, Y. Su, T. Cai, *CrystEngComm* **2022**, *24* (23), 4312–4319. DOI: <https://doi.org/10.1039/d2ce00390b>
- [9] M. Terauchi, M. Uo, Y. Fukawa, H. Yoshitake, R. Tajima, T. Ikeda, T. Yoda, *Diagnostics* **2022**, *12* (3), 651. DOI: <https://doi.org/10.3390/diagnostics12030651>
- [10] M. Reijnierse, C. Schwabl, A. Klauser, *Radiol. Clin. North Am.* **2022**, *60* (4), 641–656. DOI: <https://doi.org/10.1016/j.rcl.2022.03.007>
- [11] K. Lee, S. Lee, H. Kim, *Osteoarthritis Cartilage* **2019**, *27* (5), 781–787. DOI: <https://doi.org/10.1016/j.joca.2018.11.013>
- [12] A. Mayor, A. Tardivel, F. Martinon, V. Pe, *Nature* **2006**, *440*, 237–241. DOI: <https://doi.org/10.1038/nature04516>
- [13] O. Masala, G. Rafeletos, *Cryst. Growth Des.* **2003**, *3* (3), 431–434. DOI: <https://doi.org/10.1021/cg020064g>
- [14] M. R. Christoffersen, J. Christoffersen, *Cryst. Growth Des.* **2003**, *3* (1), 79–82. DOI: <https://doi.org/10.1021/cg025581d>
- [15] K. Ley-Ngardigal, C. Bonhomme, C. C. Diogo, P. Gras, C. Rey, *Cryst. Growth Des.* **2017**, *17*, 37–50. DOI: <https://doi.org/10.1021/acs.cgd.6b01128>
- [16] A. Wierzbicki, H. S. Cheung, *Theochem* **1998**, *454* (2–3), 287–297. DOI: [https://doi.org/10.1016/S0166-1280\(98\)00298-X](https://doi.org/10.1016/S0166-1280(98)00298-X)
- [17] F. Renaudin, S. Sarda, L. Campillo-Gimenez, C. Séverac, T. Léger, C. Charvillat, C. Rey, F. Lioté, J. M. Camadro, H. K. Ea, C. Combes, *J. Funct. Biomater.* **2019**, *10* (2), 18. DOI: <https://doi.org/10.3390/jfb10020018>
- [18] S. Polat, P. Sayan, *J. Cryst. Growth* **2021**, *562*, 126083. DOI: <https://doi.org/10.1016/j.jcrysgro.2021.126083>
- [19] F. M. Penha, A. Gopalan, J. C. Meijlink, F. Ibis, H. B. Eral, *Cryst. Growth Des.* **2021**, *21* (7), 3928–3935. DOI: <https://doi.org/10.1021/acs.cgd.1c00243>

- [20] P. Gras, C. Rey, O. Marsan, S. Sarda, C. Combes, *Eur. J. Inorg. Chem.* **2013**, 2013 (34), 5886–5895. DOI: <https://doi.org/10.1002/ejic.201300955>
- [21] F. Ibis, M. A. Nuhu, F. M. Penha, T. W. Yu, A. E. D. M. van der Heijden, H. J. M. Kramer, H. B. Eral, *Cryst. Growth Des.* **2022**, 22 (6), 3834–3844. DOI: <https://doi.org/10.1021/acs.cgd.2c00198>
- [22] S. Polat, H. B. Eral, *Adv. Powder Technol.* **2021**, 32 (10), 3650–3659. DOI: <https://doi.org/10.1016/j.apt.2021.08.021>
- [23] P. Gras, S. Teychene, C. Rey, C. Charvillat, B. Biscans, S. Sarda, C. Combes, *CrystEngComm* **2013**, 15, 2294–2300. DOI: <https://doi.org/10.1039/C2CE26499D>
- [24] N. Sbirrazzuoli, *Thermochim. Acta* **2021**, 697, 178855. DOI: <https://doi.org/10.1016/j.tca.2020.178855>
- [25] P. Budrugaec, *Thermochim. Acta* **2013**, 558, 67–73. DOI: <https://doi.org/10.1016/j.tca.2013.02.001>
- [26] T. Ozawa, *Bull. Chem. Soc. Jpn.* **1965**, 38 (11), 1881–1886.
- [27] J. H. Flynn, L. A. Wall, *Polym. Lett.* **1966**, 4, 323–328.
- [28] H. E. Kissinger, *Anal. Chem.* **1957**, 29 (11), 1702–1706.
- [29] T. Akahira, T. Sunose, *Res. Rep. Chiba Inst. Technol., Sci. Ser.* **1971**, 16, 22–31.
- [30] M. Starink, *Thermochim. Acta* **1996**, 288, 97–104. DOI: [https://doi.org/10.1016/S0040-6031\(96\)03053-5](https://doi.org/10.1016/S0040-6031(96)03053-5)
- [31] H. L. Friedman, *J. Polym. Sci., Part C: Polym. Symp.* **1964**, 6, 183–195. DOI: <https://doi.org/10.1002/polc.5070060121>
- [32] H. Kissinger, *J. Res. Natl. Bur. Stand. (U. S.)* **1956**, 57, 217–221. DOI: <https://doi.org/10.1002/9781119959809.ch9>
- [33] H. Eyring, *J. Chem. Phys.* **1935**, 3, 107–115. DOI: <https://doi.org/10.1063/1.1749604>
- [34] M. G. Evans, M. Polanyi, *Trans. Faraday Soc.* **1935**, 31, 875–894. DOI: <https://doi.org/10.1039/tf9353100875>